Anisotropic Local Correlations and Dynamics in a Relaxor Ferroelectric

Hiroyuki Takenaka, Ilya Grinberg, and Andrew M. Rappe
The Makineni Theoretical Laboratories, Department of Chemistry, University of Pennsylvania, Philadelphia, Pennsylvania 19104-6323, USA
(Received 7 August 2012; revised manuscript received 28 February 2013; published 5 April 2013)

Relaxor ferroelectrics have been a focus of intense attention due to their anomalous properties, and understanding the structure and dynamics of relaxors has been one of the long-standing challenges in solid-state physics. We investigate the local structure and dynamics in 75%$PbMg_{1/3}Nb_{2/3}O_3$-25%$PbTiO_3$ using molecular dynamics simulations and the dynamic pair distribution function technique. We show that relaxor transitions can be described by local order parameters. The relaxor phase is characterized by the presence of highly anisotropic correlations between the local cation displacements that resemble the hydrogen bond network in water. This contradicts the current model of polar nanoregion inside a nonpolar matrix. We therefore suggest a new model of a homogeneous random network of anisotropically coupled dipoles.

DOI: 10.1103/PhysRevLett.110.147602 PACS numbers: 77.80.Jk

Recently, relaxor ferroelectrics have become important in technological applications due to a strong piezoelectric effect, a high permittivity over a broad temperature range, and unique dielectric response with strong frequency dispersion, resulting in a revival of interest in this long-standing fundamental scientific problem [1–6]. The inverse dielectric response starts deviating from the Curie-Weiss law at the Burns temperature (T_b), significantly above the Curie temperature (T_c). For several decades, these effects have been ascribed to the appearance of polar nanoregions (PNRs), which form spherical or elliptic clusters in a nonpolar matrix at T_b, and increase in size due to interactions of the PNR on cooling until the Vogel-Fulcher freezing temperature (T_f). However, this model provides only a qualitative description of the changes in the structure through relaxor transitions. Furthermore, recent studies using Raman, NMR, neutron-scattering pair distribution functions (PDFs), and diffuse scattering techniques [7–11] have demonstrated that static local polarization on at least a nanosecond time scale appears only at a temperature T^* between T_c and T_f.

In this work, we use molecular dynamics (MD) simulations and analysis of PDFs for 75%$Pb(Mg_{1/3}Nb_{2/3})O_3$-25%$PbTiO_3$ (PMN-PT) to show that relaxor transitions are characterized by well-defined and observable local order parameters and are due to the onset of anisotropic nanoscale correlations of the in-phase cation motions. These correlations do not form clusters and therefore cannot be explained by the current PNR model. Rather, the couplings between displacements are analogous to the network of hydrogen bonds in water. Both in water and in relaxors, the presence of such a network in a polar environment leads to unique physical properties. We therefore propose that the PNR model should be replaced with a model of a hydrogen-bond-like network of dipoles generated by local anisotropically coupled cation displacements.

We study an 8640-atom supercell of PMN-PT with bond-valence MD simulations [12,13] in this work. Application of the dynamic pair distribution function (DPDF) method [10] enables identification of the size and directions of displacement correlations and the atomic-scale local order parameters for relaxor transitions (computational details of MD and methodology of DPDF are described in the Supplemental Material [14]).

We first compare our results with the experimental 0.75PMN-0.25PT phase transition temperatures and with integrated experimental DPDF data of Dmowski *et al.* [10] for PMN [Figs. 1(a) and 1(b)]. We integrate the total DPDF from 10 to 20 meV and from 0 to 5 meV for $2 < r < 5$ Å for our 0.75PMN-0.25PT material [Figs. 1(c) and 1(d)]. For the higher frequency interval [Fig. 1(c)], a short Pb-O peak appears at $\approx$ 550 K, same as the experimental $T_b = 550$ K of 0.75PMN-0.25PT [15]. This can be clearly seen in a 1D plot of the integrated high-frequency DPDF intensity at $r = 2.38$ Å versus temperature [Fig. 1(e)], where a more rapid rise of DPDF intensity with lower T sets in at 550 K. Though the color change in Fig. 1(d) is subtle, the 1D plot for the integrated lower-frequency DPDF intensity at $r = 3.3$ Å [Fig. 1(f)] shows two changes of slope at 550 and at 425 K. The transition at 425 K is at a temperature that is intermediate between the experimental $T_b = 550$ K and $T_f = 380$ K of 0.75PMN-0.25PT [16]. The integrated lower-frequency DPDF intensity for the short Pb-O distance [Fig. 1(d)] shows a split of the Pb-O peak away from the main Pb-O and O-O distances peak at 2.83 Å. Because the splitting decreases DPDF intensity at distances between the two peaks, we examine the integrated lower-frequency DPDF intensity for $r = 2.58$ Å [Fig. 1(g)]. This shows two changes of slope at 525 and at 350 K, with the rapid intensity decrease and strong peak splitting appearing at temperatures slightly below the experimental $T_f = 380$ K of 0.75PMN-0.25PT. Similar features are present in the integrated DPDF intensities for PMN obtained by Dmowski *et al.* [Figs. 1(a) and 1(b)]. Here, in integrated DPDF in the higher frequency interval [Fig. 1(a)], the 2.4 Å

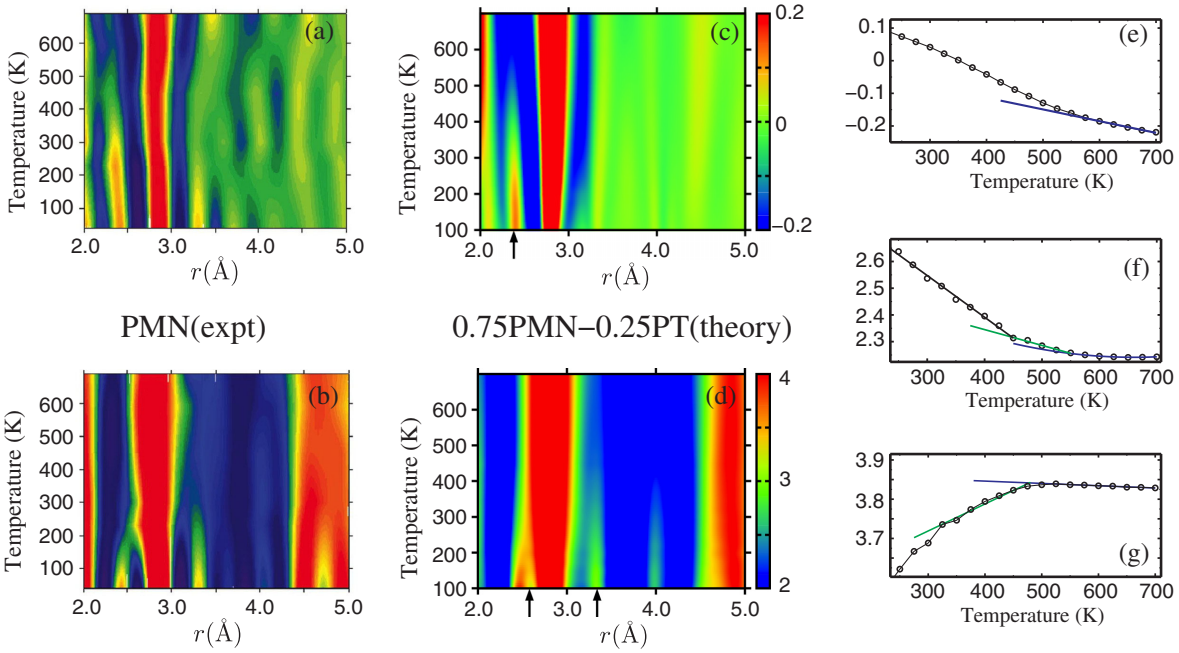

FIG. 1 (color online). The frequency averaged DPDF. (a),(b) Contour plot of experimental $G(r, \omega)$ for PMN integrated from 10 to 20 meV and from −5 to 5 meV [10]. (c),(d) Contour plot of computational 0.75PMN-0.25PT $G(r, \omega)$ integrated from 10 to 20 meV and from 0 to 5 meV, respectively. The integrated $G(r, \omega)$ are multiplied by 10^4. Arrows mark the r values for which a 1D plot of DPDF intensity versus temperature is presented in (e) integrated $G(r, \omega)$ for the high ω range at $r = 2.38$ Å, (f) for the low ω range at $r = 3.3$ Å, and (g) for low ω range at $r = 2.58$ Å. See text for interpretation of the data in the figure.

peak appears at ≈ 600 K, close to $T_b = 630$ K of PMN. In the lower frequency [Fig. 1(b)], at $r = 3.3$ Å there is a strong intensity enhancement at ≈ 300 K, between PMN $T_b = 630$ K and $T_f = 200$ K [10], and a faint increase in intensity above 300 K. The 2.4 Å peak visibly splits off from the main 2.8 Å peak at ≈ 170 K, slightly below $T_f = 200$ K. The correspondence between the transition temperatures found in our DPDF data and the experimental 0.75PMN-0.25PT values as well as the good agreement between the main features of the experimental PMN and computational 0.75PMN-0.25PT DPDFs show that our simulations are a good basis for investigating the structure and dynamics.

Cation-oxygen instantaneous and time-averaged PDFs (Fig. 2) reveal the changes in the dynamics and a sequence of transitions on cooling. The peak of the instantaneous Pb-O partial PDF $g(r, t = 0)$ presented in Fig. 2(a) corresponds to the Pb-O_{12} cage and is asymmetric for all temperatures with the positively skewed distributions of $g(r, t = 0)$ above $T = 550$ K. This means that Pb atoms shift away from the center of their O_{12} cages even in the high-temperature paraelectric phase, in agreement with previous results [12,17,18]. Unlike $g(r, t = 0)$, the time-averaged Pb-O partial PDF $G(r, \omega = 0)$ in Figure 2(b) shows almost symmetric Pb-O peaks centered at 2.81 Å for $T > 475$ K, indicating a small and temperature independent time-averaged Pb atom off centering. The strong local random fields due to the B-cation arrangement leads to the small time-averaged local cation displacements [13,17].

To clearly show the changes of local structure with temperature, we use the short Pb-O peak positions for $g(r, t = 0)$ and $G(r, \omega = 0)$ to calculate the magnitude of the instantaneous and the time-averaged static local Pb displacements ($D_{\mathrm{Pb}}^{\mathrm{inst}}$ and $D_{\mathrm{Pb}}^{\mathrm{static}}$) shown in Fig. 2(c). These are obtained by subtracting the peak position from 2.83 Å Pb-O distance of the high symmetry Pb-O_{12} cage at the 0.75PMN-0.25PT lattice constants. We also show the dynamic component of the Pb displacement $D_{\mathrm{Pb}}^{\mathrm{dyn}}$ defined as the difference between $D_{\mathrm{Pb}}^{\mathrm{inst}}$ and $D_{\mathrm{Pb}}^{\mathrm{static}}$.

Examination of the data in Fig. 2(c) shows that phase transitions occur at $T_b = 550$ K, $T^* = 450$ K, and $T_f = 375$ K; these coincide with experimental 0.75PMN-0.25PT data [15,16]. For $T > T_b$, $D_{\mathrm{Pb}}^{\mathrm{inst}}$ and $D_{\mathrm{Pb}}^{\mathrm{static}}$ are both small and change little with temperature. For $450\ \mathrm{K} < T < 550$ K, $D_{\mathrm{Pb}}^{\mathrm{inst}}$ increases rapidly as T is lowered, while $D_{\mathrm{Pb}}^{\mathrm{static}}$ is the same as for $T > 550$ K. The increasing $D_{\mathrm{Pb}}^{\mathrm{dyn}}$ indicates the onset of the dynamic relaxor phase. For $400\ \mathrm{K} < T < 450$ K, $D_{\mathrm{Pb}}^{\mathrm{static}}$ increase slowly and $D_{\mathrm{Pb}}^{\mathrm{dyn}}$ starts to plateau. Finally, at $T = 375$ K, another transition takes place with $D_{\mathrm{Pb}}^{\mathrm{static}}$ increasing rapidly and $D_{\mathrm{Pb}}^{\mathrm{dyn}}$ decreasing and both then saturating at their low temperature values, as the system undergoes a transition into the frozen phase.

The transition at T^* is characterized by the change in $D_{\mathrm{Pb}}^{\mathrm{static}}$; we therefore assign the difference between the calculated $D_{\mathrm{Pb}}^{\mathrm{static}}$ and the $D_{\mathrm{Pb}}^{\mathrm{static}}$ of the paraelectric phase as the order parameter for the low-temperature phases at $T < 475$ K. The $D_{\mathrm{Pb}}^{\mathrm{static}}$ is related to the Edwards-Anderson spin glass order parameter q, defined as $q = \Sigma_i \langle S_i \rangle^2$ [19],

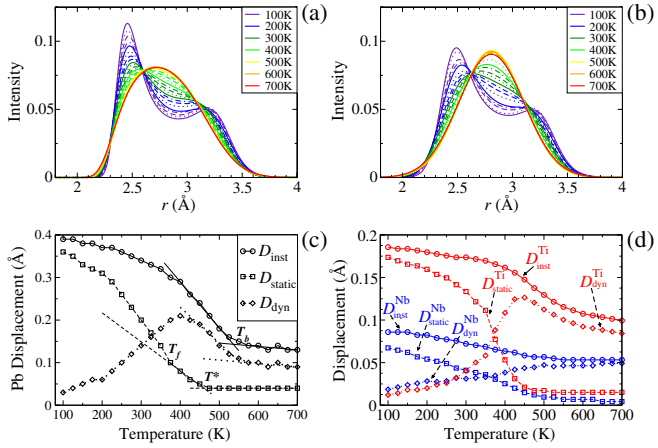

FIG. 2 (color online). Temperature dependence of instantaneous and time-averaged PDFs for cation-O atomic pairs. (a) Instantaneous $g(r, t = 0)$ and (b) time-averaged $G(r, \omega = 0)$ Pb-O partial PDFs for the first Pb-O peak. The magnitude of the instantaneous cation displacement and its static and dynamic components versus T are shown for Pb in (c) and for Nb and Ti in (d). See text for interpretation of the data in the figure.

which measures the average magnitude of the static local polarization in the material and has been used to model relaxor behavior [9,17,20]. Using NMR experiments on PMN and an analytical random-bond random-field spin model, Blinc *et al.* have previously shown that q rises above zero at a temperature between T_b and T_f [9]. This is similar to the $D^{\text{static}}_{\text{Pb}}$ rising above the paraelectric value at $T^* = 450$ K. Because q and $D^{\text{static}}_{\text{Pb}}$ *do not* change at T_b, the freezing of the local displacements that has been the focus of previous investigations is not the relevant process for the onset of relaxor behavior at T_b. Rather, the transition at T_b is characterized by the increase in the local scalar magnitude of the instantaneous cation displacements $D^{\text{inst}}_{\text{Pb}}$ [Fig. 2(c)]. We therefore assign the difference between the calculated $D^{\text{inst}}_{\text{Pb}}$ and the $D^{\text{inst}}_{\text{Pb}}$ of the paraelectric phase as the order parameter for the dynamic relaxor phase found for $\approx 475\ \text{K} < T < 550$ K.

Inspections of Nb-O and Ti-O partial PDFs [Fig. 2(d)] show trends similar to those observed for Pb displacements (Mg cation displacement magnitudes are close to zero for all temperatures). The main difference between the Pb and B-cation displacements is the D^{dyn} peaks at a higher temperature for the B cations since the cation-oxygen bonding is more distributed and flexible in the PbO_{12} cuboctahedron than in the BO_6 octahedron.

The fact that a local quantity such as Pb displacement magnitude shows order parameter behavior implies that local interactions are at the root of relaxor behavior. Enhanced local correlation between the Pb displacements is the physical origin of the increase in $D^{\text{inst}}_{\text{Pb}}$ for $T < 550$ K. Pb atom displacements in neighboring unit cells are coupled, so that correlated displacements in the same direction (even if time averaged to zero) allow a greater magnitude of individual Pb ion off centering. We now examine the cation-cation DPDFs to reveal the changes in displacement-displacement correlations that give rise to the structural and dynamical properties of the relaxor phase.

We compare Pb-Pb $G(r, \omega)$ along the (100), (110), and (111) high symmetry directions. In Fig. 3, we show only the (100) and (110) directions because the intensities along (111) directions are only slightly weaker than the intensities along (110) directions. The $G(r, \omega)$ reveal the spatial extent and the frequency spectrum of the correlated cation motion. We find that the correlations between Pb displacements are enhanced between T_f and T_b and exhibit a strong direction dependence. Starting at T_b, the $G(r, \omega)$ data along the (100) direction show a strong increase in intensity at low ω, with a shift of the low-frequency peak to below 0.1 meV as T approaches T_f. The intensity weakens and the peak position changes as r increases from 4 to 20 Å, but the appearance of low-ω peaks at T_b and their shift to lower frequencies with lower T is present for all DPDF along the (100) direction. By contrast, although the (110) and (111) directions also show peaks in the in-phase vibration intensity, they decay dramatically with increasing distance. For example, for all temperatures, we find essentially zero DPDF intensity for the (330) Pb-Pb peaks, which indicates a lack of correlated in-phase oscillations. This shows that below T_b, the coupling between the local dipoles created by Pb displacements is anisotropic, with strong interactions only between the dipoles located along Cartesian directions. Anisotropic correlations between cation displacements were also very recently reported by Akbarzadeh *et al.* in $Ba(Zr, Ti)O_3$ relaxor [20]. The direction dependences of the B-cation-B-cation correlations are more substantial and anisotropically strong coupling, confined to the B-cation sublattice, along the Cartesian directions is present even in the high temperature paraelectric phase of PMN-PT (see the Supplemental Material [14]). This is in disagreement with the current model of PNR inside a nonpolar matrix, where correlations should extend along all directions as the temperature is lowered below T_b.

The stronger correlation along the (100) direction indicates that the Pb displacement coupling is not solely due to the dipole-dipole interactions. The anisotropy is induced by the through-oxygen interactions between nearest-neighbor cations that share one (for the B cations) or more (for Pb) O atoms along a Cartesian direction in the ABO_3 structure. These interactions are stronger for the B cations, due to the much higher average bond valence of each B-cation-oxygen bond $(4/6)$ compared to the valence of the average Pb-O bond $(1/6)$. The sharing brings strong B-cation displacement coupling even in the paraelectric phase. On the other hand, for Pb atoms, the coupling along (100) is weaker and is therefore absent above T_b.

Despite the presence of strong B-cation–B-cation displacement correlations, at $T > T_b$ PMN-PT still exhibits normal paraelectric behavior. We ascribe this to the fact that the strongly correlated B-cation displacement chains are one dimensional and therefore cannot undergo

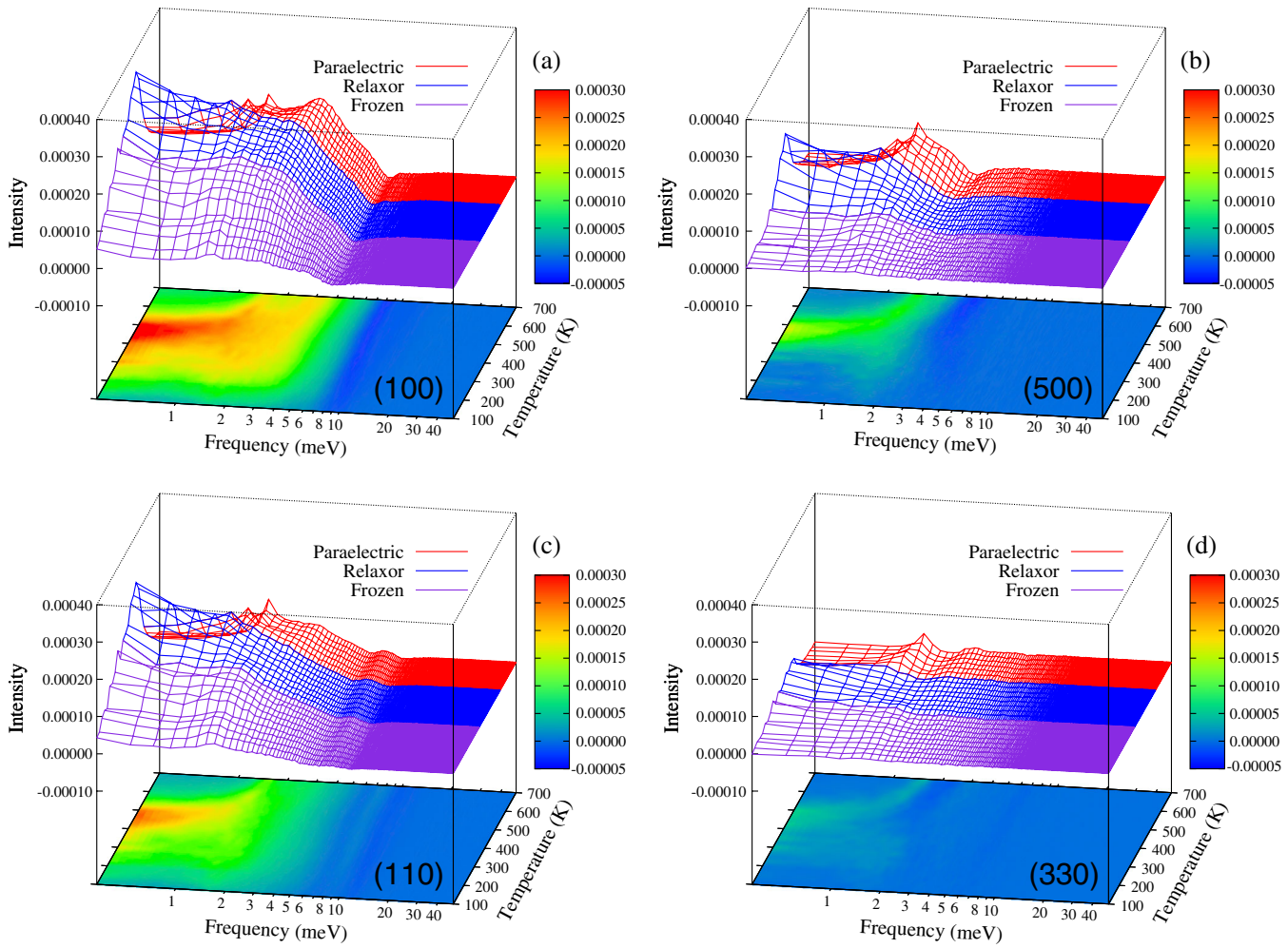

FIG. 3 (color online). Pb-Pb $G(r, \omega)$ along the high-symmetry directions as functions of temperature (K) and frequency (meV) at the peak position of the instantaneous PDF for each temperature. The contour is projected at the bottom with a color bar that shows the intensity of the peaks. Data for (a) $r = (100)$, (b) $r = (500)$, (c) $r = (110)$, and (d) $r = (330)$ are shown.

a phase transition into a more ordered phase. In addition to the through-oxygen interactions, the chains of the B-cation-B-cation correlations enhance Pb atom correlations along the Cartesian directions. At T_b, as the Pb atom displacements next to the B-cation chains become correlated, the correlated region becomes three-dimensional, enabling a transition from a paraelectric phase to a locally correlated dynamic relaxor phase.

Our results show that a network of the correlations forms a tubelike shape with a radius of around 7.5 Å, which is the same as ≈ 7 Å estimated for the size of PNR by Gehring *et al.* based on the "waterfall effect" in 0.98PZN-0.02PT [4]. The change of the correlations in the low-ω region from a sharp peak at $T > T_b$ to a broadband absorption for $T < T_b$ is in agreement with the waterfall effect observed by neutron-scattering experiments in relaxor materials. Thus, the waterfall effect stems from the correlated in-phase vibrations of cation pairs coupled by short-range through-oxygen interactions.

The in-phase vibrational correlations for low ω between a B-cation and its nearest cation show that high intensity is favored by Nb and disfavored by Mg. Especially, the Pb-Mg $G(r, \omega)$ only shows weaker changes with temperature (see Supplemental Material [14]), in contrast to all other atom pairs (including Mg-Mg). In earlier works, Mg atoms and Nb atoms surrounded by Mg atoms (Nb^{MM}) exhibited fast Arrhenius dynamics implies the high-temperature paraelectric phase even for $T < T_f$ [13,21,22]. The lack of Pb-Mg coupling causes the paraelectriclike dynamics of the Mg and Nb^{MM} atoms.

The current understanding of the relaxor transitions is that at T_b small and dynamic spherical PNR form within a paraelectric matrix; as T is lowered, the PNR grow, show smaller polarization fluctuations, and start to freeze in at T^* [11,23,24]. At T_f, a percolation transition takes place as all of the PNR coalesce into a single cluster resulting in the freezing of the local polarizations [25]. The static relaxor state is described as inhomogeneous and consisting of static PNR in a statically nonpolar matrix, with volume fraction of the PNR of about 0.3 [26].

Our results cast doubts on the conventional picture of relaxor structure and dynamics. Recent simulations have

shown that structural and dielectric properties of PMN-PT and PMN can be reproduced without PNR [13,17,27]. Relaxor behavior in Pb-based perovskites was also shown to be controlled by local structure parameters [28]. In this work, we find that the average magnitude of local cation displacements is quite large at $T \leq T_f = 375$ K, with D_{Pb} magnitude of ≈ 0.40 Å, close to that found in the prototypical normal ferroelectric $PbTiO_3$. In ferroelectric perovskites, uncorrelated displacements incur a large energy cost due to oxygen atom underbonding and overbonding, increased A-B cation repulsion, and unfavorable dipole-dipole interactions [29,30]. Therefore, a large magnitude of local polarization requires strong correlated displacements, as found in our simulations of PMN-PT; this is inconsistent with the idea that most of the material exists in a nonpolar matrix state. Additionally, we find that correlations between the cation displacements are highly anisotropic and are weak for (110) and (111) directions even at temperatures close to T_f; this is inconsistent with the picture of the strongly polarized spherical nanoclusters.

We therefore suggest an alternate model for relaxor structure and dynamics. The transition at T_b is characterized by a shift from dipole-dipole interactions to the anisotropic short-range, through-oxygen coupling along the Cartesian directions. At high T, the thermal energy is high enough to disrupt the through-oxygen coupling, so that dipole-dipole interactions play a dominant role in determining the dynamics of the system. At T_b, the energy lowering due to correlated displacements and the decrease in oxygen atom overbonding is larger than the entropy cost of correlated displacements. Therefore, the structure changes to a network of strong, through-oxygen coupled motions along the Cartesian axes. Such a transition is similar to the changes that take place when superheated water is cooled down to room temperature, where a standard polar liquid local structure dominated by dipole-dipole interactions is transformed into a directional, highly anisotropic random H-bond network with unique structural and dynamical properties. Extending an analogy suggested by Pirc and Blinc relating the ferroelectric phase to solids and the paraelectric phase to liquids [24], we suggest that relaxors are analogous to hydrogen-bonded water. A coupling network mediated by O atoms plays the role of the H bonds in water and preferential bonding directions lead to dynamic clusters of correlated displacements of various sizes. The fact that water exhibits Vogel-Fulcher dielectric response including some extremely slow relaxation processes due to the collective H-bond network behavior further supports this analogy [31].

H. T. was supported by the Department of Energy under Grant No. DE-FG02-07ER46431. I. G. was supported by the Office of Naval Research, under Grant No. N00014-12-1-1033. A. M. R. was supported by the National Science Foundation under Grant No. DMR11-24696. Computational support was provided by a Challenge Grant from the HPCMO of the U.S. Department of Defense.

[1] S.-E. Park and T. R. Shrout, J. Appl. Phys. **82**, 1804 (1997).
[2] A. S. Mischenko, Q. Zhang, R. W. Whatmore, J. F. Scott, and N. D. Mathur, Appl. Phys. Lett. **89**, 242912 (2006).
[3] Z. Kutnjak, J. Petzelt, and R. Blinc, Nature (London) **441**, 956 (2006).
[4] P. M. Gehring, S.-E. Park, and G. Shirane, Phys. Rev. Lett. **84**, 5216 (2000).
[5] R. Blinc, V. Laguta, and B. Zalar, Phys. Rev. Lett. **91**, 247601 (2003).
[6] J. F. Scott, Science **315**, 954 (2007).
[7] O. Svitelskiy, J. Toulouse, G. Yong, and Z.-G. Ye, Phys. Rev. B **68**, 104107 (2003).
[8] J. Toulouse, F. Jiang, O. Svitelskiy, W. Chen, and Z.-G. Ye, Phys. Rev. B **72**, 184106 (2005).
[9] R. Blinc, J. Dolinšek, A. Gregorovič, B. Zalar, C. Filipič, Z. Kutnjak, A. Levstik, and R. Pirc, Phys. Rev. Lett. **83**, 424 (1999).
[10] W. Dmowski, S. B. Vakhrushev, I.-K. Jeong, M. P. Hehlen, F. Trouw, and T. Egami, Phys. Rev. Lett. **100**, 137602 (2008).
[11] P. M. Gehring, S.-E. Park, and G. Shirane, Phys. Rev. B **63**, 224109 (2001).
[12] Y.-H. Shin, V. R. Cooper, I. Grinberg, and A. M. Rappe, Phys. Rev. B **71**, 054104 (2005).
[13] I. Grinberg, Y.-H. Shin, and A. M. Rappe, Phys. Rev. Lett. **103**, 197601 (2009).
[14] See Supplemental Material at http://link.aps.org/supplemental/10.1103/PhysRevLett.110.147602 for computational details of molecular dynamics simulations, methodology of the dynamic distribution function, and extra data of the correlations of in-phase motions.
[15] B. Dkhil, P. Gemeiner, A. Al-Barakaty, L. Bellaiche, E. Dul'kin, E. Mojaev, and M. Roth, Phys. Rev. B **80**, 064103 (2009).
[16] A. A. Bokov and Z.-G. Ye, Appl. Phys. Lett. **77**, 1888 (2000).
[17] M. Sepliarsky and R. E. Cohen, J. Phys. Condens. Matter **23**, 435902 (2011).
[18] M. Paściak, T. R. Welberry, J. Kulda, M. Kempa, and J. Hlinka, Phys. Rev. B **85**, 224109 (2012).
[19] S. F. Edwards and P. W. Anderson, J. Phys. F **5**, 965 (1975).
[20] A. R. Akbarzadeh, S. Prosandeev, Eric J. Walter, A. Al-Barakaty, and L. Bellaiche, Phys. Rev. Lett. **108**, 257601 (2012).
[21] I. Grinberg, H. Takenaka, Y.-H. Shin, and A. M. Rappe, J. Adv. Dielect. **2**, 1241009 (2012).
[22] S. Kamba, D. Nuzhnyy, S. Veljko, V. Bovtun, J. Petzelt, Y. L. Wang, N. Setter, J. Levoska, M. Tyunina, J. Macutkevic, and J. Banys, J. Appl. Phys. **102**, 074106 (2007).
[23] R. A. Cowley, S. N. Gvasaliya, S. G. Lushnikov, B. Roessli, and G. M. Rotaru, Adv. Phys. **60**, 229 (2011).
[24] R. Pirc and R. Blinc, Ferroelectrics **379**, 254 (2009).
[25] R. Pirc and R. Blinc, Phys. Rev. B **76**, 020101 (2007).
[26] I.-K. Jeong, T. W. Darling, J. K. Lee, T. Proffen, R. H. Heffner, J. S. Park, K. S. Hong, W. Dmowski, and T. Egami, Phys. Rev. Lett. **94**, 147602 (2005).
[27] G. G. Guzmán-Verri and C. M. Varma, arXiv:1212.3402.
[28] I. Grinberg, P. Juhás, P. K. Davies, and A. M. Rappe, Phys. Rev. Lett. **99**, 267603 (2007).
[29] I. Grinberg and A. M. Rappe, Phys. Rev. B **70**, 220101 (2004).
[30] I. Grinberg and A. M. Rappe, Phys. Rev. Lett. **98**, 037603 (2007).
[31] H. Jansson, R. Bergman, and J. Swenson, Phys. Rev. Lett. **104**, 017802 (2010).